Large Photogalvanic Spin Current by Magnetic Resonance in Bilayer Cr Trihalides

Hiroaki Ishizuka[1] and Masahiro Sato[2,3]

[1]*Department of Physics, Tokyo Institute of Technology, Meguro, Tokyo, 152-8551, Japan*
[2]*Department of Physics, Ibaraki University, Mito, Ibaraki 310-8512, Japan*
[3]*Department of Physics, Chiba University, Chiba 263-8522, Japan*

Spin current is a key to realizing various phenomena and functionalities related to spintronics. Recently, the possibility of generating spin current through a photogalvanic effect of magnons was pointed out theoretically. However, neither a candidate material nor a general formula for calculating the photogalvanic spin current in materials is known so far. In this Letter, we develop a general formula for the photogalvanic spin current through a magnetic resonance process. This mechanism involves a one-magnon excitation process in contrast to the two-particle processes studied in earlier works. Using the formula, we show that GHz and THz waves create a large photogalvanic spin current in the antiferromagnetic phase of bilayer CrI_3 and $CrBr_3$. The large spin current arises from an optical process involving two magnon bands, which is a contribution unknown to date. This spin current appears only in the antiferromagnetic ordered phase and is reversible by controlling the order parameter. These results open a route to material design for the photogalvanic effect of magnetic excitations.

Introduction.—In a photogalvanic effect, a dc electric current occurs by the illumination of light [1–3], such as in solar cells. Phenomenologically, it is a nonlinear optical effect where the current J_e reads as $J_e = \sigma^{(2)} E(\omega) E(-\omega)$. Here, $E(\omega)$ is the intensity of oscillating electric field with the frequency ω, and $\sigma^{(2)}$ is the nonlinear conductivity. This phenomenon requires inversion symmetry breaking because both J_e and $E(\omega)$ are odd under spatial inversion operation. Recent studies revealed that the photogalvanic effects are a useful probe for nontrivial electronic states such as Weyl electrons [4–9] and Berry curvature dipole [10–12]. In addition, spin [13–16] and orbital [17] currents by related mechanisms were also proposed, revealing rich nonlinear response in semiconductors.

Similar phenomena of magnetic excitations, where the spin current is generated by optically exciting magnetic excitations [18–20], have potential for optospintronics applications such as ultrafast information processing in spintronics devices [21,22]. Unlike those by electronic excitations, the spin currents by magnetic excitations occur with GHz to THz electromagnetic waves. For the photogalvanic spin current, the phenomenological formula reads as $J_s = \sigma^{(2)} h(\omega) h(-\omega)$, where J_s and $h(\omega)$ are the spin current and ac magnetic field with frequency ω, respectively. Similar to the electronic photogalvanic effect, this spin current is expected to occur in noncentrosymmetric magnets. This phenomenon is potentially beneficial for low-energy processing as the Joule heating is suppressed. However, no candidate material is known so far. Finding a material with a sufficiently large spin current density is a key for further developments in the study of photogalvanic spin current, especially for experimental studies.

In view of the symmetry requirement, bilayer trihalides are interesting candidates for studying the photogalvanic spin current. Trihalide CrI_3 is a van der Waals magnet consisting of two-dimensional honeycomb layers of Cr $S = 3/2$ spins [Fig. 1(a)]. A recent experiment discovered that a few layers of CrI_3 show magnetic orders at low temperatures, including the bilayer device [23–25]. At low temperatures, the Cr spins in each honeycomb layer align ferromagnetically, forming a ferromagnetic sheet. These ferromagnetic layers align antiferromagnetically under hydrostatic pressure [26] or by applying electric field [25,27]. Similar behavior is also known in $CrBr_3$, except that the magnetic anisotropy is weaker than CrI_3 [28]. In the paramagnetic phase, the bilayer CrI_3 has an inversion center at the middle of the two layers, whereas the antiferromagnetic order breaks the inversion symmetry [29]. Hence, a photogalvanic spin current of magnetic excitations is also allowed in the antiferromagnetic phase.

To generate a photogalvanic spin current larger than those in the previous works, we study the spin current induced by oscillating magnetic field transverse to the ordered moments. Unlike the previous studies considering oscillating longitudinal fields [19,20], we find one-magnon processes contribute to the spin current. For this purpose, we develop a general formula for the photogalvanic magnon spin current mediated by magnetic resonance. The formula consists of two contributions: the process only involving one magnon band, and the other involving two magnon bands. The two-band process related to the off-diagonal component of the spin-current operator is a contribution unknown to date, which gives a large spin
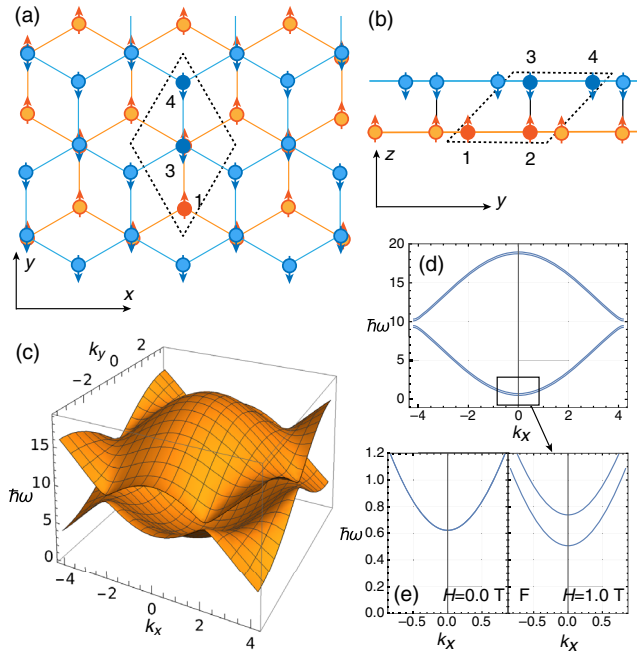
FIG. 1. Schematic of the model and its magnon dispersion. (a) and (b) are the lattice structure and magnetic order of the antiferromagnetic Cr trihalides bilayer viewed from the z and x axes, respectively. The dashed diamond is the unit cell and the numbers 1–4 denote the sublattice indices in the unit cell. (c) Magnon band structure of CrI$_3$ in the first Brillouin zone. (d) Magnon dispersion along the $k_y = 0$ line. (e),(f) Enlarged views of the lower magnon band around the Γ point with $H = 0$ T (e) and 1T (f). The parameters here are $J = 2.01$ meV, $D_z = 0.22$ meV, and $J_c = -0.59$ meV.

current in the trihalides. We find that this contribution gives the spin current conductivity $\sigma^{(2)} \sim 10^{-10}$ J cm^{-2} in bilayer CrI$_3$ and CrBr$_3$ with Gilbert damping parameter $\alpha = 10^{-2}$. This estimate is orders of magnitude larger than other proposals [19,20], reaching a value comparable to those by spinon spin Seebeck effect [30] with a 1 mT ac magnetic field. The conductivity is linearly proportional to $(\alpha\omega_0)^{-1}$ where ω_0 is the resonance frequency, implying that $\sigma^{(2)}$ increases by reducing α [31,32] or by reducing ω_0 by applying a magnetic field. The results demonstrate a theoretical prediction of photogalvanic spin current and suggest a strong candidate material for experimental studies.

Spin model for Cr trihalides.—The effective spin model for bulk CrI$_3$ consists of layered honeycomb lattices of $S = 3/2$ Cr spins. The exchange interaction and anisotropy of the Cr spins are estimated from the inelastic neutron-scattering experiment [33], wherein the authors find a dominant intralayer nearest-neighbor Heisenberg interaction and uniaxial anisotropy, along with other small intralayer interactions. Hence, we consider an effective spin Hamiltonian with the nearest-neighbor ferromagnetic interaction J, interlayer antiferromagnetic interaction J_c, and the easy-axis anisotropy D_z.

The Hamiltonian reads as

$$H_0 = -J \sum_{\langle in, jm \rangle} \boldsymbol{S}_{in} \cdot \boldsymbol{S}_{jm} - J_c \sum_i \boldsymbol{S}_{i2} \cdot \boldsymbol{S}_{i3}$$
$$- D_z \sum_{in} (S_{in}^z)^2 - h \sum_{in} S_{in}^z, \qquad (1)$$

where $\boldsymbol{S}_{in} \equiv (S_{in}^x, S_{in}^y, S_{in}^z)$ is the $S = 3/2$ Heisenberg spin on the sublattice $n = 1, \ldots, 4$ of the ith unit cell. Sublattices $n = 1, 2$ form the first honeycomb layer, and $n = 3, 4$ sublattices form the second one. The final term is the Zeeman interaction with an external static field $h = g\mu_B H$ ($g \simeq 2$ is the g factor, μ_B is the Bohr magneton, and H is an applied static magnetic field along the z axis). The fitting of magnon bands to neutron scattering data gives $J = 2.01$ meV, $D_z = 0.22$ meV, and $J_c = 0.59$ meV [33]. The interlayer coupling in this estimate is ferromagnetic because the antiferromagnetic phase appears only by applying gate voltage or by applying pressure. As the magnetic transition temperature in the antiferromagnetic phase is almost the same as that of the ferromagnetic phase, we assume $J_c = -0.59$ meV in the antiferromagnetic phase. With this negative J_c, the ground state is an antiferromagnetically ordered state with the two ferromagnetic honeycomb layers aligning in an antiparallel configuration [Fig. 1(a)]. Here, the spins point along the z axis due to the uniaxial anisotropy D_z. The effective Hamiltonian for CrBr$_3$ is similar to the CrI$_3$ Hamiltonian except for the values of the exchange interactions and the anisotropy [34,35], as we will discuss later; most importantly, the anisotropy is smaller in CrBr$_3$.

To study the photoinduced dynamics in our model H_0 with reasonable accuracy, we apply the spin-wave theory. Details of the calculation are elaborated upon in the Supplemental Material [36]. Figures 1(c)–1(f) show the magnon band $\omega_{n\vec{k}}$ in the antiferromagnetic phase of CrI$_3$ using the above parameters. Here, $\vec{k} = (k_x, k_y)$ is the wave vector of magnons and n is the band index. The magnon bands are doubly degenerate at $h = 0$, while a finite field h lifts the degeneracy due to the Zeeman splitting [Fig. 1(f)]. The calculated band structure is in semiquantitative agreement with the recent experiment [38].

Spin current conductivity.—To generate a photoinduced dc spin current, we apply an ac transverse field to the system H_0, whose Hamiltonian is given by

$$H'(t) = -h_x(t) \sum_{i,n} S_{in}^x - h_y(t) \sum_{i,n} S_{in}^y, \qquad (2)$$

where t is time and $h_a(t)$ ($a = x, y$) are the ac magnetic field along x and y axes. We note that this light-matter coupling is distinct from those in Refs. [19,20], where the magnetic field couples to S_{in}^z.

The nonlinear spin current conductivity $[\sigma^{(2)}]^\alpha_{\mu\nu\lambda}(0;\omega,-\omega)$ for the perturbation, Eq. (2), is defined by [39]

$$J^\alpha_\mu(0) = \sum_{\mu,\nu} \int [\sigma^{(2)}]^\alpha_{\mu\nu\lambda}(0;\omega,-\omega)h_\nu(\omega)h_\lambda(-\omega)d\omega, \qquad (3)$$

where $\mathcal{J}^z_\mu = \sum_{\langle in,jm\rangle} J[(r_j)_\mu - (r_i)_\mu](S^x_{in}S^y_{jm} - S^y_{in}S^x_{jm})$ is the spin current for the α component of spin angular momentum flowing along the μ axis, $J^\alpha_\mu(\Omega) = \int \langle \mathcal{J}^\alpha_\mu\rangle e^{-i\Omega t}dt$ is the Fourier transform of thermal average of the spin current $\mathcal{J}^\alpha_\mu$, and $h_\mu(\omega) = \int h_\mu(t)e^{-i\omega t}dt$ is the Fourier transform of $h_\mu(t)$. Here, only J^z_μ is discussed; as S^z is a conserved quantity, we can define this spin current unambiguously from the continuity equation.

To accurately estimate $\sigma^{(2)}(0;\omega,-\omega)$, we derive the generic formula for the second-order nonlinear conductivity by the ac transverse field. The detailed derivation of the formula is given in the Supplemental Material [36]. Utilizing the formula, we compute the dc spin current conductivity $\sigma^{(2)}$ of our model $H_0 + H'(t)$.

Figure 2 shows the frequency ω dependence of $[\sigma^{(2)}]^z_{yxx}(0;\omega,-\omega)$ for the antiferromagnetic phase of the model in Eq. (1); the magnon relaxation rate reads as $1/\tau = \alpha\omega$ where $\alpha = 10^{-2}$ is the Gilbert damping constant. We only show the results for $[\sigma^{(2)}]^z_{yxx}$ as $[\sigma^{(2)}]^z_{yyy}$ is the same as $[\sigma^{(2)}]^z_{yxx}$, and $[\sigma^{(2)}]^z_{xxy}$ is zero due to the symmetry of CrI$_3$ (see Supplemental Material [36] for details). The position of two peaks in Fig. 2(a) corresponds to the frequency of magnons at $\vec{k} = 0$ in Fig. 1(d). The conductivity at the resonance peaks in Fig. 2 are $\sigma^{(2)} \sim 10^{-11}$ J cm^{-2} T^{-2}, and is linearly proportional to τ. Previous theories [19,20] argue that $J_s \sim 10^{-16}$ J cm^{-2} is necessary for the experimental observation of spin current. According to Fig. 2, ~ 1 mT ac magnetic field ($\sim 10^3$–10^4 V cm^{-1}) is required to produce $J_s \sim 10^{-16}$ J cm^{-2} for $\tau = 1/\alpha\omega_0 = 6.62 \times 10^{-10}$ s. The required ac magnetic field is a couple of orders smaller than that of the mechanism in previous works [19,20].

In Fig. 2(b), we show the magnetic field dependence of $[\sigma^{(2)}]^z_{y\nu\lambda}(0;\omega,-\omega)$. The resonance frequency of the lower peak at zero static field is in the order of 10^2 GHz, which is a consequence of the magnon gap induced by the single-ion anisotropy of CrI$_3$. Each peak split into two under the static magnetic field, reflecting the lifting of the degeneracy of magnon bands. By increasing the magnetic field, the lower band eventually reaches zero energy causing a transition to a ferromagnetic phase. The field-induced antiferromagnetic to ferromagnetic transition at $H \sim 0.5$–1.0 T is indeed observed in the experiment [26,27]. Hence, the resonance frequency can be tuned by the external magnetic field within experimentally available field strength.
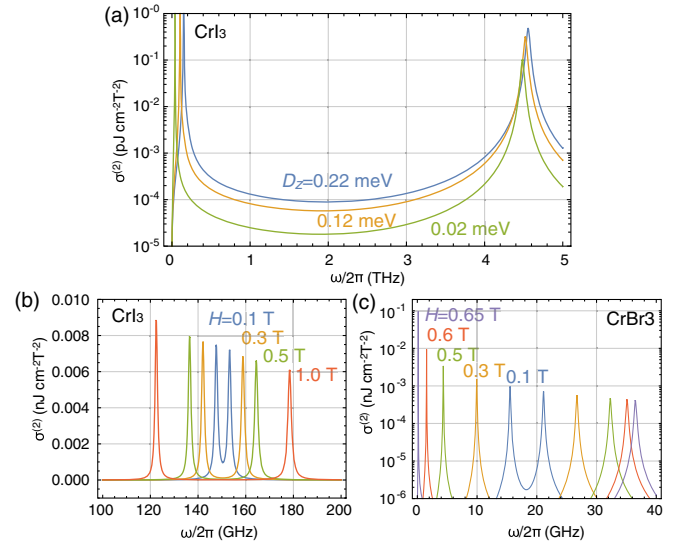

FIG. 2. Spin current conductivity $[\sigma^{(2)}]^z_{yxx}(0;\omega,-\omega)$ for the model in Eq. (1) with Gilbert damping $\alpha = 10^{-2}$. (a) Frequency dependence of the spin current conductivity for different anisotropy $D_z = 0.22$ meV (blue), 0.12 meV (orange), and 0.02 meV (green). The data for $D_z = 0.22$ meV corresponds to CrI$_3$. Other parameters are $J = 2.01$ meV, $J_c = -0.59$ meV, and $D_z = 0.04$ meV. (b) Frequency dependence of the lower peaks for the static magnetic field $H = 0.1$ T (blue), 0.3 T (orange), 0.5 T (green), and 1.0 T (red). (c) Frequency dependence of the lower peaks for CrBr$_3$ with $H = 0.1$ T, 0.3 T, 0.5 T, 0.6 T, and 0.65 T. The data are for $J = 1.36$ meV, $J_c = -0.024$ meV, and $D_z = 0.04$ meV.

Another route to tune the magnon gap is by changing the anisotropy. A recent study reports that Cr trihalides with different halide ions have different anisotropy [28,40]: CrI$_3$ is an easy-axis type magnet, whereas CrBr$_3$ is almost Heisenberg-like with a small single-ion anisotropy, and the magnetic moments in CrCl$_3$ are XY-like. In addition, the interlayer coupling of CrBr$_3$ is controllable between ferromagnetic and antiferromagnetic by controlling the stacking [41]. As in Fig. 2(a), the peak position for the antiferromagnetic order shifts to lower frequency as D_z decreases. In Fig. 2(c), we show the H dependence of $[\sigma^{(2)}]^z_{yxx}(0;\omega,-\omega)$ for CrBr$_3$, in which the parameters are estimated as $J = 1.36$ meV, $J_c = -0.024$ meV, and $D_z = 0.04$ meV [34,35]. The results are qualitatively the same as that of CrI$_3$ in Fig. 2(b), except that the resonance frequency is lower. The peak $[\sigma^{(2)}]^z_{yxx}(0;\omega,-\omega)$ increases rapidly reflecting the low resonance frequency which diverges as it approaches zero; the result for $H = 0.65$ T is 2 orders of magnitude larger than that of $H = 0.1$ T [see Fig. 2(c)]. Hence, as discussed below, reducing the resonance frequency by a magnetic field is a route to further enhance the spin current.

Two-band process.—We next turn to the mechanism of the photogalvanic response by the ac transverse field.

TABLE I. List of mechanisms for photoinduced spin current by Zeeman coupling. FM stands for ferromagnet and PGSC is for photogalvanic spin current. The last column shows the direction of the external ac field: longitudinal (transverse) is for the field along (perpendicular to) the ordered moment. All setups assume a magnetic order except for the spinon PGSC.

	Mechanism	Material	Spin current	Ac field
Spin pump [42]	Magnetic resonance	FM	Diffusion	Transverse
Spinon PGSC [19]	Two-spinon excitation	Noncentrosymmetric spin chain	Shift current	Longitudinal
Magnon PGSC [20]	Two-magnon excitation	Noncentrosymmetric magnet	Shift current	Longitudinal
One-band magnon PGSC [18]	Magnetic resonance + single-band process	Helical magnet with DM interaction	Injection current	Transverse
Two-band magnon PGSC [this paper]	Magnetic resonance + two-band process	Noncentrosymmetric magnet	Injection current	Transverse

The general formula in the Supplemental Material [36] consists of two single-magnon excitation terms

$$[\sigma^{(2)}]_{\mu\nu\lambda}^z(0;\omega,-\omega) = [\sigma^{(2;1b)}]_{\mu\nu\lambda}^z(0;\omega,-\omega) \\ + [\sigma^{(2;2b)}]_{\mu\nu\lambda}^z(0;\omega,-\omega), \qquad (4)$$

$$[\sigma^{(2;1b)}]_{\mu\nu\lambda}^z(0;\omega,-\omega) = -\mathrm{i}\frac{\tau}{\pi}\sum_{m=1}^{n_{\mathrm{uc}}}\left[\frac{\tilde{\beta}_m^\nu[(\tilde{J}_{\vec{0}}^\mu)_{m,m}]\tilde{\beta}_{m+n_{\mathrm{uc}}}^\lambda}{\omega-\omega_{m\vec{0}}-\mathrm{i}/2\tau} \\ + \frac{\tilde{\beta}_m^\lambda[(\tilde{J}_{\vec{0}}^\mu)_{m,m}]\tilde{\beta}_{m+n_{\mathrm{uc}}}^\nu}{\omega+\omega_{m\vec{0}}-\mathrm{i}/2\tau}\right],$$

$$[\sigma^{(2;2b)}]_{\mu\nu\lambda}^z(0;\omega,-\omega) = -\frac{1}{2\pi}\sum_{\substack{m,l=1\\m\neq l}}^{n_{\mathrm{uc}}}\frac{1}{\omega_{m\vec{0}}-\omega_{l\vec{0}}-\mathrm{i}/2\tau} \\ \times\left[\frac{\tilde{\beta}_l^\nu[(\tilde{J}_{\vec{0}}^\mu)_{l,m}+(\tilde{J}_{\vec{0}}^\mu)_{m+n_{\mathrm{uc}},l+n_{\mathrm{uc}}}]\tilde{\beta}_{m+n_{\mathrm{uc}}}^\lambda}{\omega-\omega_{l\vec{0}}-\mathrm{i}/2\tau} \\ + \frac{\tilde{\beta}_l^\lambda[(\tilde{J}_{\vec{0}}^\mu)_{l,m}+(\tilde{J}_{\vec{0}}^\mu)_{m+n_{\mathrm{uc}},l+n_{\mathrm{uc}}}]\tilde{\beta}_{m+n_{\mathrm{uc}}}^\nu}{\omega+\omega_{m\vec{0}}-\mathrm{i}/2\tau}\right],$$

where $\tilde{J}_{\vec{0}}^\mu$ is the $2n_{\mathrm{uc}}\times 2n_{\mathrm{uc}}$ matrix of the spin current operator in the magnon eigenstate basis ($n_{\mathrm{uc}}=4$ is the number of sublattices), $\omega_{m\vec{k}}$ is the eigenfrequency of the mth magnon band with the momentum $\vec{k}$, and $\tilde{\beta}_l^\mu$ is the coupling constant between h_μ ($\mu=x,y$) and the lth $\vec{k}=\vec{0}$ magnon. The formal definition of $\tilde{J}_{\vec{0}}$ and $\tilde{\beta}_l^\mu$ is given in the Supplemental Material along with the derivation of the formula. The first term in Eq. (4), $[\sigma^{(2;1b)}]_{\mu\nu\lambda}^z(0;\omega,-\omega)$, is the contribution that involves one magnon band whereas the second term, $[\sigma^{(2;2b)}]_{\mu\nu\lambda}^z(0;\omega,-\omega)$, involves two magnon bands (Table I). Unlike the previous work, however, there are no two-magnon terms in the excitation by ac transverse field, as the transverse field does not couple to two-magnon terms [36].

Among the two terms in Eq. (4), the two-band contribution $[\sigma^{(2;2b)}]_{\mu\nu\lambda}^z(0;\omega,-\omega)$ does not require Dzyaloshinskii-Moriya (DM) interaction. The one-band contribution is proportional to the diagonal component of the spin current operator, hence, to the group velocity of magnons at $\vec{k}=\vec{0}$. Therefore, DM interaction is necessary for the one-band process as studied in a previous work [18]. In contrast, the two-band contribution is related to the off-diagonal components of the spin-current operator. These terms generally remain nonzero at $\vec{k}=\vec{0}$ regardless of the symmetry of the band. Therefore, the two-band process contributes to the photogalvanic spin current in a system with symmetric dispersion $\omega_{m\vec{k}}=\omega_{m,-\vec{k}}$, in contrast to the one-band process.

We re-emphasize that two-particle processes similar to those in Refs. [19,20] do not exist in Eq. (4). Hence, only single-particle processes contribute to the spin current. The difference of the microscopic mechanism manifests as the relaxation time dependence: the two-magnon mechanism is shift-current-like ($\sigma^{(2)}\propto\tau^0$) whereas the present proposal is injection-current-like ($\sigma^{(2)}\propto\tau^1$). These differences are summarized in Table I. As we discussed above, the one-magnon process produces a spin current orders of magnitude larger than the previous estimates for two-particle excitation processes. At the resonance frequency $\omega=\omega_{m\vec{0}}$, the two-band process is dominated by the resonating magnon band, and the conductivity is given by

$$[\sigma^{(2;2b)}]_{\mu\nu\lambda}^z \sim -\mathrm{i}\frac{\tau}{\pi}\sum_{\substack{l=1\\l\neq m}}^{n_{\mathrm{uc}}}\frac{1}{\omega_{m\vec{0}}-\omega_{l\vec{0}}-\mathrm{i}/2\tau} \\ \times [\tilde{\beta}_m^\nu[(\tilde{J}_{\vec{0}}^\mu)_{m,l}+(\tilde{J}_{\vec{0}}^\mu)_{l+n_{\mathrm{uc}},m+n_{\mathrm{uc}}}]\tilde{\beta}_{l+n_{\mathrm{uc}}}^\lambda \\ + \tilde{\beta}_l^\lambda[(\tilde{J}_{\vec{0}}^\mu)_{l,m}+(\tilde{J}_{\vec{0}}^\mu)_{m+n_{\mathrm{uc}},l+n_{\mathrm{uc}}}]\tilde{\beta}_{m+n_{\mathrm{uc}}}^\nu]. \qquad (5)$$

The spin current is proportional to τ, and hence, it is like the injection current in the photogalvanic effect. This formula also implies that $[\sigma^{(2;2b)}]_{\mu\nu\lambda}^z$ increases linearly with $\tau=(\alpha\omega_{m\vec{0}})^{-1}$. Hence, a smaller resonance frequency is favorable as in Fig. 2(c).

Discussion.—In this Letter, we developed a general theory for the photogalvanic spin current induced by ac transverse magnetic field. Unlike the previous work finding

only a two-magnon process producing the spin current [20], the photogalvanic spin current by the ac transverse field occurs through one-magnon processes. Using this formula, we study the spin current in bilayer CrI$_3$, in which we find a large nonlinear spin current conductivity in its antiferromagnetic phase. The conductivity shows sharp peaks at the frequency corresponding to the energy of $\vec{k} = \vec{0}$ magnon modes. At the resonance frequency, the peak reaches $\sigma \sim 10^{-10}$ J cm^{-2} T^{-2} for $\alpha = 10^{-2}$ despite the small magnetic-field component of the electromagnetic wave, several orders of magnitude larger than that produced by other mechanisms [19,20]. The estimated conductivity implies a spin current of $J_s \sim 10^{-16}$ J cm^{-2} created by 1 mT ac magnetic field. The larger response due to a new mechanism implies a larger response is generally possible by the single-magnon process.

Recent studies on Cr trihalides revealed that they are highly controllable two-dimensional magnets where both ferromagnetic and antiferromagnetic phases are realized. Our calculation shows that the photogalvanic spin current appears in the antiferromagnetic phase, whereas it is prohibited in the ferromagnetic phase. For the experiment, a setup similar to that in ferromagnetic resonance studies should suffice [43,44]. In addition, the direction of spin current changes depending on the orientation of the antiferromagnetic order, i.e., whether the magnetic moments on the first and second layers are an up-down or down-up type. This directional nature is inherently different from that of spin pumping [42], in which photo-induced spin current diffusively expands to all directions. These properties of the photogalvanic spin current delineate themselves from similar phenomena.

Generating spin current in different frequency regimes is important for experiments and applications because different techniques are used for different frequencies. For instance, intense THz fields are often generated using lasers [45,46], whereas the GHz fields utilize electronics technologies. Each technique has its strengths and weaknesses, which play critical roles in designing experiments and devices. Therefore, extending the frequency range in which the photogalvanic spin current occurs extends the opportunities for experiments and applications.

Optical technologies in the GHz to THz domain have experienced significant progress over recent years. GHz waves have been long used in magnetic resonance experiments [47], and THz laser pulse techniques have been developed in the last decades [45,46]. In spintronics [22,48], such techniques are utilized to control magnetic states [21]. Intense-THz-laser-driven phenomena in magnets have also been explored experimentally [49–51] and theoretically [52–55]. The photogalvanic spin current proposed in this work should be detectable using the currently available techniques of GHz-THz waves.

[1] B. I. Sturman and V. M. Fridkin, *The Photovoltaic and Photorefractive Effects in Noncentrosymmetric Materials* (Gordon and Breach, Philadelphia, 1992).

[2] L. Z. Tan, F. Zheng, S. M. Young, F. Wang, S. Liu, and A. M. Rappe, Shift current bulk photovoltaic effect in polar materials-hybrid and oxide perovskites and beyond, npj Comput. Mater. **2**, 16026 (2016).

[3] Y. Tokura and N. Nagaosa, Nonreciprocal responses from non-centrosymmetric quantum materials, Nat. Commun. **9**, 3740 (2018).

[4] H. Ishizuka, T. Hayata, M. Ueda, and N. Nagaosa, Emergent Electromagnetic Induction and Adiabatic Charge Pumping in Noncentrosymmetric Weyl Semimetals, Phys. Rev. Lett. **117**, 216601 (2016).

[5] C.-K. Chan, N. H. Lindner, G. Refael, and P. A. Lee, Photocurrents in Weyl semimetals, Phys. Rev. B **95**, 041104(R) (2017).

[6] F. de Juan, A. G. Grushin, T. Morimoto, and J. E. Moore, Quantized circular photogalvanic effect in Weyl semimetals, Nat. Commun. **8**, 15995 (2017).

[7] Q. Ma, S.-Y. Xu, C.-K. Chan, C.-L. Zhang, G. Chang, Y. Lin, W. Xie, T. Palacios, H. Lin, S. Jia, P. A. Lee, P. Jarillo-Herrero, and N. Gedik, Direct optical detection of Weyl fermion chirality in a topological semimetal, Nat. Phys. **13**, 842 (2017).

[8] G. B. Osterhoudt, L. K. Diebel, M. J. Gray, X. Yang, J. Stanco, X. Huang, B. Shen, N. Ni, P. J. W. Moll, Y. Ran, and K. S. Burch, Colossal mid-infrared bulk photovoltaic effect in a type-I Weyl semimetal, Nat. Mater. **18**, 471 (2019).

[9] D. Rees, K. Manna, B. Lu, T. Morimoto, H. Borrmann, C. Felser, J. E. Moore, D. H. Torchinsky, and J. Orenstein, Helicity-dependent photocurrents in the chiral Weyl semimetal RhSi, Sci. Adv. **6**, eaba0509 (2020).

[10] J. E. Moore and J. Orenstein, Confinement-Induced Berry Phase and Helicity-Dependent Photocurrents, Phys. Rev. Lett. **105**, 026805 (2010).

[11] I. Sodemann and L. Fu, Quantum Nonlinear Hall Effect Induced by Berry Curvature Dipole in Time-Reversal Invariant Materials, Phys. Rev. Lett. **115**, 216806 (2015).

[12] S.-Y. Xu, Q. Ma, H. Shen, V. Fatemi, S. Wu, T.-R. Chang, G. Chang, A. M. Mier Valdivia, C.-K. Chan, Q. D. Gibson, J. Zhou, Z. Liu, K. Watanabe, T. Taniguchi, H. Lin, R. J. Cava, L. Fu, N. Gedik, and P. Jarillo-Herrero, Electrically switchable Berry curvature dipole in the monolayer topological insulator WTe$_2$, Nat. Phys. **14**, 900 (2018).

[13] S, M. Young, F. Zheng, and A. M. Rappe, Prediction of a Linear Spin Bulk Photovoltaic Effect in Antiferromagnets, Phys. Rev. Lett. **110**, 057201 (2013).

[14] R. Fei, W. Song, L. Pusey-Nazzaro, and L. Yang, *PT*-Symmetry-Enabled Spin Circular Photogalvanic Effect in Antiferromagnetic Insulators, Phys. Rev. Lett. **127**, 207402 (2021).

[15] H. Xu, H. Wang, J. Zhou, and J. Li, Pure spin photocurrent in non-centrosymmetric crystals: Bulk spin photovoltaic effect, Nat. Commun. **12**, 4330 (2021).

[16] E. V. Boström, T. S. Parvini, J. W. Iverer, A. Rubio, S. V. Kusminskiy, and M. A. Sentef, All-optical generation of antiferromagnetic magnon currents via the magnon circular photogalvanic effect, Phys. Rev. B **104**, L100404 (2021).

[17] M. Davydova, M. Serbyn, and H. Ishizuka, Nonlinear orbital response across topological phase transition in centrosymmetric materials, Phys. Rev. B **105**, L121407 (2022).

[18] I. Proskurin, A. S. Ovchinnikov, J.-I. Kishine, and R. L. Stamps, Excitation of magnon spin photocurrents in antiferromagnetic insulators, Phys. Rev. B **98**, 134422 (2018).

[19] H. Ishizuka and M. Sato, Theory for shift current of bosons: Photogalvanic spin current in ferrimagnetic and antiferromagnetic insulators, Phys. Rev. B **100**, 224411 (2019).

[20] H. Ishizuka and M. Sato, Rectification of Spin Current in Inversion-Asymmetric Magnets with Linearly Polarized Electromagnetic Waves, Phys. Rev. Lett. **122**, 197702 (2019).

[21] P. Nemec, M. Fiebig, T. Kampfrath, and A. V. Kimel, Antiferromagnetic opto-spintronics, Nat. Phys. **14**, 229 (2018).

[22] V. Baltz, A. Manchon, M. Tsoi, T. Moriyama, T. Ono, and Y. Tserkovnyak, Antiferromagnetic spintronics, Rev. Mod. Phys. **90**, 015005 (2018).

[23] M. A. McGuire, H. Dixit, V. R. Cooper, and B. C. Sales, Coupling of crystal structure and magnetism in the layered, ferromagnetic insulator CrI_3, Chem. Mater. **27**, 612 (2015).

[24] B. Huang, G. Clark, E. Navarro-Moratalla, D. R. Klein, R. Cheng, K. L. Seyler, D. Zhong, E. Schmidgall, M. A. McGuire, D. H. Cobden, W. Yao, D. Xiao, P. Jarillo-Herrero, and X. Xu, Layer-dependent ferromagnetism in a van der Waals crystal down to the monolayer limit, Nature (London) **546**, 270 (2017).

[25] T. Song, X. Cai, M. W.-Y. Tu, X. Zhang, B. Huang, N. P. Wilson, K. L. Seyler, L. Zhu, T. Taniguchi, K. Watanabe, M. A. McGuire, D. H. Cobden, D. Xiao, W. Yao, and X. Xu, Giant tunneling magnetoresistance in spin-filter van der Waals heterostructures, Science **360**, 1214 (2018).

[26] T. Li, S. Jiang, N. Sivadas, Z. Wang, Y. Xu, D. Weber, J. E. Goldberger, K. Watanabe, T. Taniguchi, C. J. Fennie, K. F. Mak, and J. Shan, Pressure-controlled interlayer magnetism in atomically thin CrI_3, Nat. Mater. **18**, 1303 (2019).

[27] S. Jiang, J. Shan, and K. F. Mak, Electric-field switching of two-dimensional van der Waals magnets, Nat. Mater. **17**, 406 (2018).

[28] H. H. Kim, B. Yang, S. Li, S. Jiang, C. Jin, Z. Tao, G. Nichols, F. Sfigakis, S. Zhong, C. Li, S. Tian, D. G. Cory, G.-X. Miao, J. Shan, K. F. Mak, H. Lei, K. Sun, L. Zhao, and A. W. Tsen, Evolution of interlayer and intralayer magnetism in three atomically thin chromium trihalides, Proc. Natl. Acad. Sci. U.S.A. **116**, 11131 (2019).

[29] Y. Zhang, T. Holder, H. Ishizuka, F. de Juan, N. Nagaosa, C. Felser, and B. Yan, Switchable magnetic bulk photovoltaic effect in the two-dimensional magnet CrI_3, Nat. Commun. **10**, 3738 (2019).

[30] D. Hirobe, M. Sato, T. Kawamata, Y. Shiomi, K. Uchida, R. Iguchi, Y. Koike, S. Maekawa, and E. Saitoh, One-dimensional spinon spin currents, Nat. Phys. **13**, 30 (2017).

[31] K. Lenz, H. Wende, W. Kuch, K. Baberschke, K. Nagy, and A. Jánossy, Two-magnon scattering and viscous Gilbert damping in ultrathin ferromagnets, Phys. Rev. B **73**, 144424 (2006).

[32] C. Vittoria, S. D. Yoon, and A. Widom, Relaxation mechanism for ordered magnetic materials, Phys. Rev. B **81**, 014412 (2010).

[33] L. Chen, J.-H. Chung, B. Gao, T. Chen, M. B. Stone, A. I. Kolesnikov, Q. Huang, and P. Dai, Topological Spin Excitations in Honeycomb Ferromagnet CrI_3, Phys. Rev. X **8**, 041028 (2018).

[34] E. J. Samuelsen, R. Silberglitt, G. Shirane, and J. P. Remeika, Spin waves in ferromagnetic $CrBr_3$ studied by inelastic neutron scattering, Phys. Rev. B **3**, 157 (1971).

[35] Z. Cai, S. Bao, Z.-L. Gu, Y.-P. Gao, Z. Ma, Y. Shangguan, W. Si, Z.-Y. Dong, W. Wang, Y. Wu, D. Lin, J. Wang, K. Ran, S. Li, D. Adroja, X. Xi, S.-L. Yu, X. Wu, J.-X. Li, and J. Wen, Topological magnon insulator spin excitations in the two-dimensional ferromagnet $CrBr_3$, Phys. Rev. B **104**, L020402 (2021).

[36] See Supplemental Material at http://link.aps.org/supplemental/10.1103/PhysRevLett.129.107201, which includes Ref. [37] for the derivation of general formula.

[37] J. H. P. Corpa, Diagonalization of the quadratic boson hamiltonian, Physica (Amsterdam) **93A**, 327 (1978).

[38] J. Cenker, B. Huang, N. Suri, P. Thijssen, A. Miller, T. Song, T. Taniguchi, K. Watanabe, M. A. McGuire, D. Xiao, and X. Xu, Direct observation of two-dimensional magnons in atomically thin CrI_3, Nat. Phys. **17**, 20 (2021).

[39] W. Kraut and R. von Baltz, Anomalous bulk photovoltaic effect in ferroelectrics: A quadratic response theory, Phys. Rev. B **19**, 1548 (1979).

[40] C. Bacaksiz, D. Šabani, R. M. Menezes, and M. V. Milošević, Distinctive magnetic properties of CrI_3 and $CrBr_3$ monolayers caused by spin-orbit coupling, Phys. Rev. B **103**, 125418 (2021).

[41] W. Chen, Z. Sun, Z. Wang, L. Gu, X. Xu, S. Wu, and C. Gao, Direct observation of van der Waals stackingdependent interlayer magnetism, Science **366**, 983 (2019).

[42] Y. Kajiwara, K. Harii, S. Takahashi, J. Ohe, K. Uchida, M. Mizuguchi, H. Umezawa, H. Kawai, K. Ando, K. Takanashi, S. Maekawa, and E. Saitoh, Transmission of electrical signals by spin-wave interconversion in a magnetic insulator, Nature (London) **464**, 262 (2010).

[43] I. Lee, F. G. Utermohlen, D. Weber, K. Hwang, C. Zhang, J. van Tol, J. E. Goldberger, N. Trivedi, and P. C. Hammel, Fundamental Spin Interactions Underlying the Magnetic Anisotropy in the Kitaev Ferromagnet CrI_3, Phys. Rev. Lett. **124**, 017201 (2020).

[44] J. Zeisner, K. Mehlawat, A. Alfonsov, M. Roslova, T. Doert, A. Isaeva, B. Büchner, and V. Kataev, Electron spin resonance and ferromagnetic resonance spectroscopy in the high-field phase of the van der Waals magnet $CrCl_3$, Phys. Rev. Mater. **4**, 064406 (2020).

[45] H. Hirori, A. Doi, F. Blanchard, and K. Tanaka, Single-cycle terahertz pulses with amplitudes exceeding 1 MV/cm

generated by optical rectification in LiNbO3, Appl. Phys. Lett. **98,** 091106 (2011).

[46] B. Liu, H. Bromberger, A. Cartella, T. Gebert, M. Först, and A. Cavalleri, Generation of narrowband, high-intensity, carrier envelope phase-stable pulses tunable between 4 and 18 THz, Opt. Lett. **42,** 129 (2017).

[47] C. P. Slichter, *Principles of Magnetic Resonance* (Springer, Berlin, 1990).

[48] *Spin Current*, 2nd ed., edited by S. Maekawa, S. O. Valenzuela, E. Saitoh, and T. Kimura (Oxford University Press, Oxford, 2017).

[49] T. Kubacka *et al.*, Large-amplitude spin dynamics driven by a THz pulse in resonance with an electromagnon, Science **343,** 1333 (2014).

[50] Y. Mukai, H. Hirori, T. Yamamoto, H. Kageyama, and K. Tanaka, Nonlinear magnetization dynamics of antiferromagnetic spin resonance induced by intense terahertz magnetic field, New J. Phys. **18,** 013045 (2016).

[51] J. Lu, X. Li, H. Y. Hwang, B. K. Ofori-Okai, T. Kurihara, T. Suemoto, and K. A. Nelson, Coherent Two-Dimensional Terahertz Magnetic Resonance Spectroscopy of Collective Spin Waves, Phys. Rev. Lett. **118,** 207204 (2017).

[52] M. Mochizuki and N. Nagaosa, Theoretically Predicted Picosecond Optical Switching of Spin Chirality in Multiferroics, Phys. Rev. Lett. **105,** 147202 (2010).

[53] M. Sato, S. Takayoshi, and T. Oka, Laser-Driven Multiferroics And Ultrafast Spin Current Generation, Phys. Rev. Lett. **117,** 147202 (2016).

[54] M. Sato and Y. Morisaku, Two-photon driven magnon-pair resonance as a signature of spin-nematic order, Phys. Rev. B **102,** 060401(R) (2020).

[55] M. Kanega, T. N. Ikeda, and M. Sato, Linear and nonlinear optical responses in Kitaev spin liquids, Phys. Rev. Research **3,** L032024 (2021).